Nanocomposites

DOI: 10.1002/anie.200801064

Amorphous Silica Nanoparticles Embedded in Epitaxial $SrTiO_3$ and $CoFe_2O_4$ Matrices**

Hongmei Luo, Yuan Lin, Haiyan Wang, Scott A. Baily, Joon Hwan Lee, Marilyn E. Hawley, T. Mark McCleskey, Anthony K. Burrell, Eve Bauer, Leonardo Civale, and Quanxi X. Jia**

Silica (SiO_2)–metal oxide composites have a wide range of potential applications in many fields such as catalysis, sensors, optics, magnetism, and electronics. For example, SiO_2 or mesoporous SiO_2 are often used as insulating matrices or supports for metal oxide nanoparticles for catalytic and sensor applications.[1–3] The addition of SiO_2 can enhance the coercivity of $CoFe_2O_4$ (CFO) in SiO_2-CFO powders or CFO thin films grown on silicon or silica substrates.[4–13] Furthermore, SiO_2 can enhance the magnetoresistance in SiO_2–$La_{0.7}Sr_{0.3}MnO_3$ composites.[14] SiO_2 not only affects the magnetic properties of magnetic materials but also modifies the electrical properties of oxides. For instance, SiO_2 has been used to enhance the dielectric constants of $ZrSiO_4$ and $HfSiO_4$.[15] In addition, SiO_2–ZrO_2, SiO_2–HfO_2, and SiO_2–$SrTiO_3$ (STO) composites have been investigated as possible replacements for SiO_2 as the gate dielectric materials in standard complementary metal-oxide-semiconductor (CMOS) transistors.[16–19] It should be noted that most efforts in this field have involved incorporating SiO_2 into metal oxide powders or metal oxide polycrystalline films. The composites are commonly prepared by the sol–gel method using tetraethoxysilane (TEOS, $Si(OC_2H_5)_4$) as the silica source.

Herein we report SiO_2 nanoparticles with grain sizes as small as 10 nm embedded in epitaxial STO and CFO matrices prepared by a solution approach involving polymer-assisted deposition (PAD).[20,21] The water-soluble polymer controls the desired viscosity and binds the metal ions to prevent premature precipitation, which results in a homogeneous distribution of the metal ions in solution and the formation of uniform metal oxide thin films. Solutions of different metals can be mixed to control the stoichiometry when preparing complex metal oxides. We found that SiO_2 nanoparticles bind to polyethyleneimine (PEI) polymer presumably by a surfactant-like interaction of the polymer with the surface of the nanoparticles. The ease of forming the soluble SiO_2 nanoparticle solution makes it very attractive as a precursor to SiO_2-metal oxide composite films. Herein we have selected STO and CFO to explore this unique synthetic route to nanocomposite materials.

As compared to LAO (pseudo-cubic with a lattice constant a of 0.3789 nm), STO is cubic with $a = 0.3905$ nm, while CFO possesses a face-centered-cubic inverse spinel structure with $a = 0.838$ nm ($a/2 = 0.419$ nm). Such small lattice mismatches make it possible to grow both STO and CFO epitaxially on LAO substrates. An analysis of the X-ray diffraction (XRD) θ–2θ scans indicates that only STO and CFO (001) peaks are present, with no peaks attributable to silica, thereby indicating that silica retains its amorphous nature in the composite films. Figure 1 displays the ϕ-scans

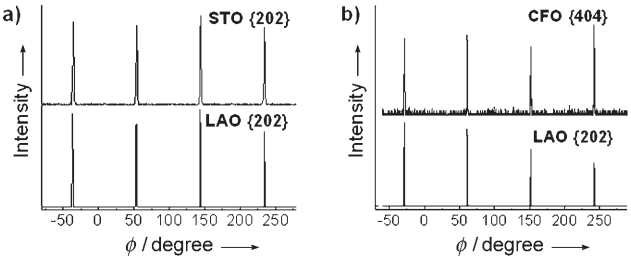

Figure 1. XRD ϕ-scans for a SiO_2–STO (10:90) composite film from the (202) reflections of STO and LAO (a), and an SiO_2–CFO (30:70) composite film from the (202) reflection of LAO and the (404) reflection of CFO (b).

from the reflections of LAO {202} and STO {202} for SiO_2–STO (10:90) and LAO {202} and CFO {404} for SiO_2–CFO (30:70) composite films. The epitaxial relationship between the substrate and the matrices (STO and CFO) can be described as $(001)_{film}||(001)_{LAO}$ and $[101]_{film}||[101]_{LAO}$. It should be noted that the epitaxial quality for SiO_2–STO and SiO_2–CFO composite films is quite good, with an average full width at half maximum (FWHM) value of 1.0° for STO and 0.8° for CFO, as compared to 0.6° for the single-crystalline LAO substrate.

Figure 2 shows the atomic force microscopy (AFM) phase images of the same SiO_2–STO and SiO_2–CFO composite films on LAO substrates. These images clearly show silica nanoparticles (round white dots) with sizes of about 10 nm randomly dispersed in the STO matrix. The surfaces of the films are quite smooth with a root mean square (rms) surface roughness of about 1.8 nm for SiO_2–STO and about 4.7 nm for SiO_2–CFO. As the annealing temperature is higher for SiO_2–

[*] Dr. H. M. Luo, Dr. Y. Lin, Dr. S. A. Baily, Dr. M. E. Hawley, Dr. T. M. McCleskey, Dr. A. K. Burrell, E. Bauer, Dr. L. Civale, Dr. Q. X. Jia
Experimental Physical Sciences, Los Alamos National Laboratory, Los Alamos, NM 87545 (USA)
Fax: (+1) (505) 665-3164
E-mail: hluo@lanl.gov
qxjia@lanl.gov
Dr. H. Wang, J. H. Lee
Department of Electrical and Computer Engineering, Texas A&M University, College Station, TX 77843-3128 (USA)

[**] We gratefully acknowledge the support of the U.S. Department of Energy (DOE) through the LANL/LDRD Program, the DOE EE-RE Solid State Lighting Program, and the NSF/DMR Ceramic Program (NSF 0709831).

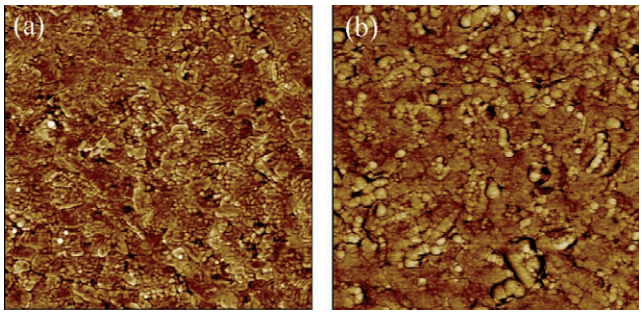

Figure 2. AFM phase images of a) an SiO_2–STO (10:90) composite film ($2\times2\ \mu m^2$) and b) an SiO_2–CFO (30:70) composite film ($1\times1\ \mu m^2$).

CFO, the silica nanoparticles become larger (≥ 20 nm) due to the merging of individual nanoparticles.

Figures 3 a and b show cross-section high-resolution transmission electron microscopy (HRTEM) images of an SiO_2–STO (10:90) film on a LAO substrate from two different areas. The images clearly indicate that the STO phase has grown epitaxially on the LAO substrate and that SiO_2 grains of about 10 nm are embedded randomly in the epitaxial STO matrix. From a materials science point of view, it is very interesting to note that there are two different epitaxial growth mechanisms taking place in these nanocomposites: vertical heteroepitaxy happens where the epitaxial matrix is in contact with the substrate, and lateral homoepitaxy occurs over the top of amorphous nanoparticles. The corresponding

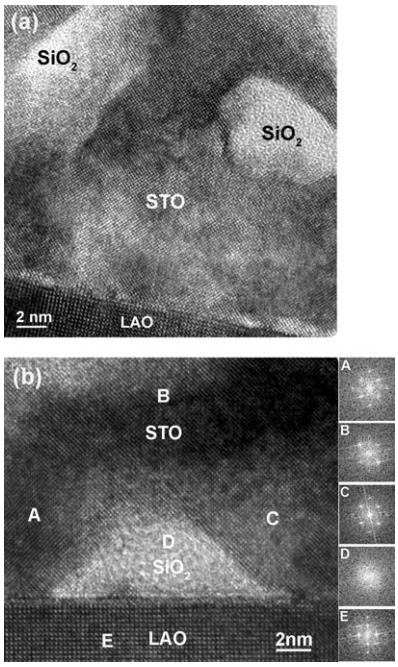

Figure 3. Cross-section HRTEM images of a) amorphous SiO_2 nanoparticles in an epitaxial STO matrix, and b) vertical heteroepitaxy, when STO is in direct contact with the substrate, and lateral homoepitaxy, when STO is on the top of amorphous particles. The corresponding Fast Fourier Transform (FFT) images taken at different spots (A, B, C, and E) indicate epitaxy being established in the ferroelectric material matrix; the FFT image of spot D shows the amorphous nature of SiO_2.

Fast Fourier Transform (FFT) images on different spots (A, B, C, and E) indicate epitaxy being established in the STO matrix. This, to the best of our knowledge, is the first successful attempt to grow such amorphous nanoparticles in an epitaxial matrix based on a chemical solution approach.

Figure 4 shows the cross-section HRTEM images and the corresponding selected area electron diffraction (SAED) patterns for an SiO_2-CFO (30:70) film on LAO. Similar to the

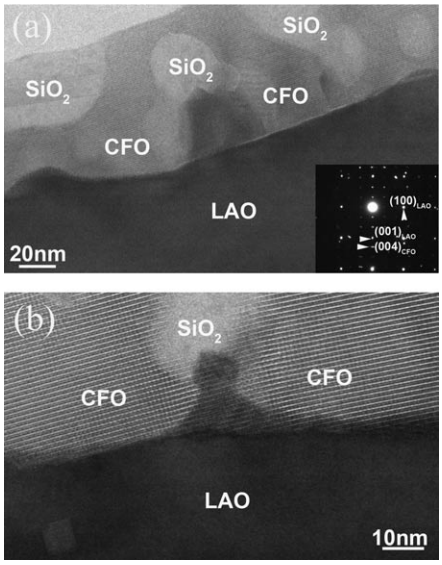

Figure 4. a,b) Cross-section HRTEM images of an SiO_2–CFO (30:70) composite film on an LAO substrate and the corresponding SAED pattern (inset) taken from the interface between the film and the substrate.

SiO_2–STO composites, CFO has grown epitaxially on the substrate, with amorphous silica nanoparticles embedded inside the epitaxial matrix. It is evident that the silica nanoparticles increase in size with annealing temperature, from around 10 nm in STO films annealed at 860 °C to more than 20 nm in CFO films annealed at 950 °C. However, the amorphous SiO_2 nanoparticles do not disrupt the epitaxial growth of STO or CFO phases on the substrate. It is noted that the combination of heteroepitaxial growth (in direct contact with the substrate) and homoepitaxial growth (on the top of the amorphous regions) has been used to manipulate the strain state in the epitaxial growth of (Ba,Sr)TiO_3 (BST) or GaN films with amorphous stripes pre-patterned on the substrate.[22,23] This suggests that SiO_2 nanoparticles in our nanocomposite films can potentially be used to fine-tune the strain state of the epitaxial matrix.

In an effort to explore the effect of silica on the magnetic properties of CFO, we have investigated SiO_2–CFO composite films with varying amounts of SiO_2. In this experiment, all films were subjected to the same annealing process and had a thickness of 150 nm; their ferrimagnetic properties were evaluated with a superconducting quantum interference device magnetometer (SQUID). Figure 5 shows the magnetization versus magnetic field (M–H) hysteresis loops with magnetic field parallel to the substrate surface measured at

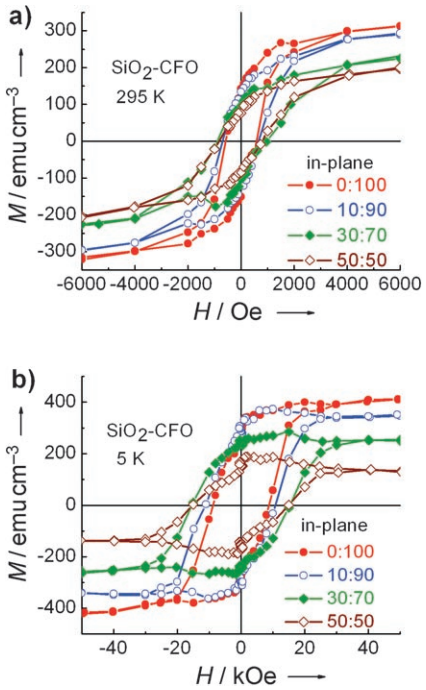

Figure 5. Magnetization versus magnetic field (*M*–*H*) hysteresis loops with the magnetic field parallel to the substrate surface at a) 295 and b) 5 K for pure CFO and SiO_2–CFO (10:90, 30:70, and 50:50) composite films.

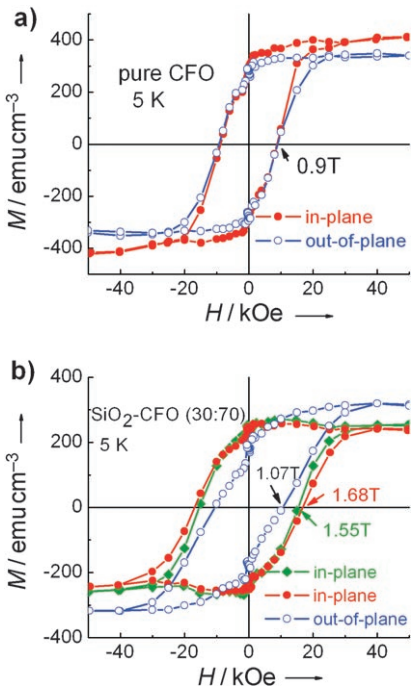

Figure 6. Magnetization versus magnetic field (*M*–*H*) hysteresis loops with the magnetic field parallel and perpendicular to the substrate surface at 5 K for a) pure CFO and b) SiO_2–CFO (30:70) composite films. The green line is the in-plane measurement of the film before removing SiO_2, and the red and blue lines are the in-plane and out-of-plane measurements for the film after removing SiO_2.

295 and 5 K for SiO_2–CFO films with compositions of 0:100 (pure CFO), 10:90, 30:70, and 50:50, respectively. The saturation and remanent magnetization of the composites decrease with increasing amounts of SiO_2, which is consistent with dilution of the magnetic CFO phase using nonmagnetic silica. The coercivity of the films is 570, 680, and 920 Oe at 295 K when the amount of SiO_2 is 0, 10, and 30, respectively. The coercivity decreases to a value of 820 Oe when the SiO_2 amount is 50. At 5 K, the coercivity follows the same trend but with larger absolute values of 0.9, 1.1, 1.55, and 1.5 T, respectively.

It is well known that silica can be etched off by treatment with HF or NaOH at room temperature. Thus, porous epitaxial oxide thin films are expected to be formed upon removing the silica from silica-metal oxide composite films. However, we should point out that it is likely that only the silica nanoparticles on the top surface region can be removed unless the silica content is high enough to connect these amorphous particles. It is more interesting to note that the pores affect the magnetic properties as well. Figure 6 shows the *M*–*H* hysteresis loops with magnetic fields parallel and perpendicular to the substrate surface at 5 K for pure CFO and SiO_2-$CoFe_2O_4$ (30:70) films (before and after removing silica with HF). For the pure CFO film, both the in-plane and out-of-plane loops have similar shapes with the same coercivity of 0.9 T, which illustrates that magnetic anisotropy is not evident in a pure CFO film. We can therefore consider the film to be isotropic. However, the porous film shows magnetic anisotropy, with an in-plane coercivity of 1.68 T and an out-of-plane coercivity of 1.07 T. As CFO and SiO_2 have very different lattice parameters and thermal coefficients, the presence of a relatively large lattice strain and the separation of CFO crystallites by nonmagnetic SiO_2 may lead to magnetic anisotropy and high coercivity.[6,9,10] Compared to the composite film before removing silica, the porous film shows a slight increase of the in-plane coercivity from 1.55 to 1.68 T. It is reasonable to expect a higher coercivity for porous materials considering the domain wall pinning caused by the non-uniform porous structures. For example, mesoporous Co films and Ni porous networks show coercivities of between 100 to 300 Oe, compared to 10 Oe for bulk Co and about 90 Oe for dense Co films.[24,25]

Experimental Section

Sample preparation: The precursor solutions for the deposition of SiO_2–metal oxide (e.g. STO and CFO) composite films were obtained from a mixture of separate solutions of silica and the corresponding metals (e.g. Sr and Ti solutions for STO, Co and Fe solutions for CFO). The Sr binds to polyethyleneimine (PEI) polymer as an ethylenediaminetetraacetic acid (EDTA) complex when using Sr-$(NO_3)_2$ as the metal precursor, Ti binds to carboxylated-polyethyleneimine (PEIC) with $TiCl_4$ as the precursor,[20] and Co and Fe bind to PEI when using $CoCl_2$ and $FeCl_3$ as precursors. Commercial Ludox silica nanoparticles with sizes of around 10 nm bind to PEI. Both PEI and EDTA were purchased from BASF Corporation of Clifton, NJ, and were used without further purification. Ultrafiltration and concentration were carried out under 60 psi nitrogen using Amicon stirred cells that have a cut-off molecular weight of 3000. Metal analysis was conducted using a Varian Liberty 220 inductively coupled plasma-atomic emission spectrometer (ICP-AES) following the standard SW846 EPA (Environmental Protection Agency)

Method 6010 procedure. The final concentrations of Sr, Ti, Co, Fe, and silica were 157, 408, 295, 209, and 460 mM, respectively. The resulting precursor solutions were spin-coated onto the $LaAlO_3$ (LAO) substrates with SiO_2-to-STO molar ratios of 0:100 and 10:90, and SiO_2-to-CFO molar ratios of 0:100, 10:90, 30:70, and 50:50. The precursor SiO_2-STO and SiO_2-CFO films were annealed in flowing oxygen for 2 h at 860 and 950 °C, respectively.

Sample characterizations: X-ray diffraction (XRD) was used to characterize the crystallographic orientation of the films. The microstructure of the films was analyzed by transmission electron microscopy (TEM). The surface morphology and surface roughness of the films were analyzed by scanning electron microscopy (SEM) and atomic force microscopy (AFM). The ferrimagnetic properties of the films were evaluated with a superconducting quantum interference device magnetometer (SQUID).

Received: March 5, 2008
Published online: June 23, 2008

Keywords: magnetic properties · materials science · nanocomposites · silica · thin films

[1] R. Tongpool, S. Jindasuwan, *Sens. Actuators B* **2005**, *106*, 523 – 528.
[2] C. Cantalini, M. Post, D. Buso, M. Guglielmi, A. Martucci, *Sens. Actuators B* **2005**, *108*, 184 – 192.
[3] H.-J. Kim, Y.-G. Shul, H. Han, *Top. Catal.* **2005**, *35*, 287 – 293.
[4] S. R. Mekala, J. Ding, *J. Alloys Compd.* **2000**, *296*, 152 – 156.
[5] J. Ding, Y. J. Chen, Y. Shi, S. Wang, *Appl. Phys. Lett.* **2000**, *77*, 3621 – 3623.
[6] J. Ding, H. Gong, R. Melaka, S. Wang, Y. Shi, Y. J. Chen, N. X. Phuc, *J. Magn. Magn. Mater.* **2001**, *226–230*, 1382 – 1384.
[7] X. H. Huang, Z. H. Chen, *Solid State Commun.* **2004**, *132*, 845 – 850.
[8] X. H. Huang, Z. H. Chen, *J. Cryst. Growth* **2004**, *271*, 287 – 293.
[9] Y. C. Wang, J. Ding, J. B. Yi, B. H. Liu, T. Yu, Z. X. Shen, *Appl. Phys. Lett.* **2004**, *84*, 2596 – 2598.
[10] J. H. Yin, J. Ding, B. H. Liu, Y. C. Wang, J. B. Yi, J. S. Chen, X. S. Miao, *IEEE Trans. Magn.* **2005**, *41*, 3904 – 3906.
[11] J. Vejpravová, J. Plocek, D. Nižňanský, A. Hutlová, J. L. Rehspringer, V. Sechovský, *IEEE Trans. Magn.* **2005**, *41*, 3469 – 3471.
[12] C. Cannas, A. Musinu, D. Peddis, G. Piccaluga, *Chem. Mater.* **2006**, *18*, 3835 – 3842.
[13] A. Casu, M. F. Casula, A. Corrias, A. Falqui, D. Loche, S. Marras, *J. Phys. Chem. C* **2007**, *111*, 916 – 922.
[14] Y.-H. Huang, C.-H. Yan, S. Wang, F. Luo, Z.-M. Wang, C.-S. Liao, G.-X. Xu, *J. Mater. Chem.* **2001**, *11*, 3296 – 3299.
[15] G. Lucovsky, Jr., G. B. Rayner, *Appl. Phys. Lett.* **2000**, *77*, 2912 – 2914.
[16] D. A. Neumayer, E. Cartier, *J. Appl. Phys.* **2001**, *90*, 1801 – 1807.
[17] T. S. Böscke, S. Govindarajan, P. D. Kirsch, P. Y. Hung, C. Krug, B. H. Lee, J. Heitmann, U. Schröder, G. Pant, B. E. Gnade, W. H. Krautschneider, *Appl. Phys. Lett.* **2007**, *91*, 072902.
[18] H.-Y. Chou, T.-M. Chen, T.-Y. Tseng, *J. Phys. D* **2005**, *38*, 2446 – 2451.
[19] C.-C. Lin, L.-W. Lai, C.-Y. Lin, T.-Y. Tseng, *Thin Solid Films* **2007**, *515*, 8005 – 8008.
[20] A. K. Burrell, T. M. McCleskey, Q. X. Jia, *Chem. Commun.* **2008** 1271 – 1277.
[21] Q. X. Jia, T. M. McCleskey, A. K. Burrell, Y. Lin, G. E. Collis, H. Wang, A. D. Q. Li, S. R. Foltyn, *Nat. Mater.* **2004**, *3*, 529 – 532.
[22] J.-S. Lee, H. Wang, S. Y. Lee, S. R. Foltyn, Q. X. Jia, *Appl. Phys. Lett.* **2003**, *83*, 5494 – 5496.
[23] C. I. H. Ashby, C. C. Mitchell, J. Han, N. A. Missert, P. P. Provencio, D. M. Follstaedt, G. M. Peake, L. Griego, *Appl. Phys. Lett.* **2000**, *77*, 3233 – 3235.
[24] H. M. Luo, L. Sun, Y. F. Lu, Y. S. Yan, *Langmuir* **2004**, *20*, 10218 – 10222.
[25] L. Sun, C. L. Chien, P. C. Searson, *Chem. Mater.* **2004**, *16*, 3125 – 3129.

